AN IMPURITY BEAM-TRAPPING INSTABILITY IN TOKAMAKS *

J. T. Hogan and H. C. Howe

CONF-760209--12

ABSTRACT

We consider the sensitivity of neutron energy production to the impurity trapping of injected neutral beams. This process is affected by inherent low-Z contamination of the tritium pre-heat plasma, by the species composition of the neutral beam, and by the entrance angle of the beam. We compare the sensitivities of the process to these variables, and to the variation of wall material. We find that successful use of a low-Z, low-sputtering material can appreciably lengthen the useful pulse length.

AN IMPURITY BEAM-TRAPPING INSTABILITY IN TOKAMAKS

I. INTRODUCTION

Plasma-surface interactions play an important role in all present CTR devices [1, 2]. With the advent of high power levels of neutral beam heating [3, 4], where $P_{injected} \geq P_{ohmic}$, new considerations also require detailed understanding of plasma/surface effects and may impose more stringent requirements on materials.

The conventional view of the problems posed by impurity contaminants is that the radiative losses which they cause may impose impossibly high requirements for plasma τ_E values [4]. Neoclassical transport theory predicts that impurities will accumulate in the core, so that heavy metals used in the wall or limiter may cause substantial energy losses even at elevated temperature. This is viewed as a serious problem for thermonuclear power reactors, which should operate with pulse lengths many times longer than an energy confinement time in order to produce high values of Q (≡ fusion output/energy input). An analysis of the energy deposition-impurity production cycle may be schematized as in Figure 1: there is a natural time delay which allows the production of small amounts of energy ($Q \gtrsim 1$) before impurity effects predominate. Thus experiments such as the Tokamak Fusion Test Reactor (TFTR) near plasma break-even conditions should be feasible.

This conventional view must be modified when intensely beam-driven tokamaks are considered. While ohmic heating energy may be preferentially deposited in high-resistivity plasma regions, the energy input through fast-ion thermalization must be reconsidered.

Rome, et al. [5] have treated the beam-deposition problem. They find that for ratios of plasma minor radius to mean free path $(a/\lambda_o) \leq 1/4$, the beam energy will be deposited in the plasma core. The mean free path is computed from several beam trapping processes

a) Charge exchange by protons (deuterons, tritons) and impurity ions,

b) Impact ionization by protons (deuterons, tritons) and impurity ions.

Cross sections for trapping by hydrogenic particles are given by Riviere [6] and Freeman [7]. The influence of impurities in beam trapping has been suggested by Girard, et al [8] and Furth [9].

It is the impurity trapping process which we must consider. For injection experiments now underway, or planned, rough typical values range from $a/\lambda_c \sim 1/3$ (ORMAK, ORMAK upgrade), to ~ 1 (PLT), to 1.3 (TFTR, full-radius). We see that attainment of $a/\lambda_o \leq 1/4$ may be difficult. If this is true, the beam will be trapped closer to the plasma edge than had been supposed. When the fast ions thermalize, and heat the edge region with its higher neutral density, the charge exchange bombardment will be more intense than the flux from the core considered in [1]. Thus, more impurities will be produced, a/λ will increase even more, the beam will be trapped even closer to the edge, and an instability will occur which eventually prevents further beam penetration.

To describe the requirements on materials which this new process imposes, we shall first discuss the models that we employ

for the plasma and wall. We then take up the dynamics of the beam trapping instability, and then discuss the sensitivity of the process to the choice of materials.

II. MODELS FOR PLASMA AND WALL PROCESSES

We use a transport code which computes the radial and temporal evolution of the plasma and impurity temperatures and densities. (See Reference 10 for a review.) The plasma transport and injection models are described elsewhere [11,12]. The neutral gas is treated with an analytic [1] transport model. The beam processes are treated with moments of the Fokker-Planck equation [13] or by direct solution of the Fokker-Planck equation. The energy balance includes thermal conduction and convection processes, charge exchange, line radiation, bremsstrahlung and recombination losses, input from the thermalization of fast injection particles and alpha particles. The particle balance accounts for diffusive losses and input by ionization of neutrals, thermalized injected particles and electrons produced by the stripping of impurity ions.

We describe processes which are of special interest in the plasma-wall interaction more fully:

1. Impurity properties: The important plasma transport variables are

a) $$Z_{eff} \equiv \frac{\sum N_k Z_k^2}{N_e}$$

b) $$[Z] \equiv \frac{\sum N_k Z_k^2 N_p/N_k}{N_e}$$

c) $N_f \equiv N_e - \sum_k N_k Z_k$

d) Q_{low}: Radiation from 'low Z' impurities ($Z \leq 30$)

e) Q_{high}: Radiation from 'high Z' impurities ($Z > 30$)

2. Charge exchange losses: The plasma profiles are computed self-consistently and lead to a spectrum of outgoing neutrals which is a function of energy and angle (E, θ).

The normal incidence sputtering yield is multiplied by $1/\cos\theta$ and integrated with $f_{CX}(E, \theta)$ to obtain a $\bar{Y}(E)$. This result is integrated to obtain a net sputtering yield over all energies and angles. Figure 2 shows results for a fixed T_i profile (unlike calculations presented later) in which we vary the machine size. One sees that

$$\bar{\bar{Y}} \equiv \frac{\int d^3v \; v_\perp \; f_{CX}(\underline{v}) \; \bar{Y}(E)}{\int d^3v \; v_\perp \; f_{CX}(\underline{v}) \; E} \qquad (\#/eV)$$

is a slowly varying function of size. Detailed calculations of the emergent spectra are needed for interpretation of experiments, and will yield needed information for experiments such as ISX and TEXTOR. For the purposes of this sensitivity study we will characterize the sputtering produced by the plasma-wall interaction in terms of a fixed number ($\bar{\bar{Y}}$) of impurity ions per eV of emergent charge exchange loss.

3. Impurity diffusion: We treat neoclassical impurity diffusion in the Pfirsch-Schluter regime [14]

$$[1] \quad \frac{\partial}{\partial t} N_Z = \frac{1}{r} \frac{\partial}{\partial r} (r \Gamma_Z) + \Sigma_Z$$

where Γ_Z and Σ_Z are the flux and source of impurity ions, respectively. We assume that all ions produced by sputtering

are deposited in the outermost spatial cell of the computation. We treat the relative distribution of charge states by means of the coronal equilibria calculated by Jordan [15].

4. Beam-impurity effects:

a) Cross section for trapping. As we have noted, there exists some probability that the impact ionization process for beam-impurity collisions will be the dominant effect at energies of interest for thermonuclear plasmas. We assume that the beam trapping along the path of a beam line [5] is given by

$$\frac{dn_b}{ds} = - n_b \left(\sigma_{CX}\, n_i + Z^2\, \sigma_i\, n_Z + \sigma_i\, n_i\right) \tag{2}$$

where Z, n_Z are the impurity charge and density. $\sigma_{CX,i}$ are the charge exchange and fuel ion (H, D, or T) impact ionization cross sections. $n_{b,i,e}$ are the beam, fuel ion and electron densities.

b) Thermalization. During thermalization the fast ions scatter in pitch-angle at a rate proportional to $\langle Z_{eff} \rangle$. This does not affect the energy deposition to the background. The fast ions transfer energy primarily to electrons when their energy $W \geq E_{crit}$, where

$$E_{crit} = 14.8\, T_e\, M_b \left[\frac{[Z]}{M_f}\right]^{2/3} M_{b,f} \tag{3}$$

$M_{b,f}$: mass of beam, fuel ions. Thus, a heavy admixture of low-Z impurities can shift the heating to the electrons by lowering [Z] and hence E_{crit}.

c) Radial dependence. The fast-ion lifetime τ_f varies by a large factor from the plasma core to the corona. This effect strongly influences the beam trapping instability, for the metabolism of the impurity production cycle is enhanced if energy is delivered to the plasma more quickly.

III. BEAM TRAPPING INSTABILITY

To show the instability in clear-cut form we examine a beam-driven system. We choose a tokamak with the dimensions of TFTR, and choose beam power levels which are those envisaged for the device. Figure 3 shows the results of the evolution of this instability. We assume that charge exchange sputtering of the wall (iron) is the dominant impurity production process.

1. Evolution of the instability:

We assume the plasma (100% T) has been pre-heated to 4 keV and isolated from the wall. The current is at 1 MA at t = 0 and injection starts at 20 milliseconds. The subsequent heating is shown in Fig. 3a. In the course of the plasma free expansion from its' initial isolated position, a 'cold plasma blanket' is formed which is helpful in reducing impurity inward migration [16] (Fig. 3b). The iron impurities manage to 'tunnel through' this blanket, however, and eventually reach the plasma core (Fig. 3c). The beam-deposition properties are measured by the function H(r)[5] which is normalized so that its volume integral is unity. In Fig. 3d we see the time

evolution of H(r) (for the full energy component of the beams) as the beam deposition moves out. As the injected beam is assumed to have full, half, and third energy components present in the ratio 1:2:1, we show the time evolution of H(0) for all components in Fig. 3e. The output of the TFTR is shown in Fig. 3f, where attainment of neutron energies 1 MJ/pulse is achieved in spite of the instability. At 300 milliseconds, however, temperatures and Q are decreasing, so that this process could not be extrapolated to longer times in a power-producing reactor.

We note that Q is defined for the entire injection pulse, and that for selected intervals of time within this pulse $Q \sim 1$ experiments may be performed.

2. Variation with pre-heating impurity content:

The presence of significant amounts of low-Z impurities, such as oxygen, can produce an early onset of the beam-exclusion process. Figures 4a,b show a comparison between cases with initial oxygen content leading to Z_{eff} of 3 and 6, respectively. These bracket the current experimental range. While the neutron energy production is not greatly affected, the cleaner case shows substantially higher ion temperature and a longer useful pulse.

3. Variation with beam energy composition:

If the species in the D^0 neutral beams can be controlled, significant improvement will be obtained. Fig. 5a,b show a case with the 1:2:1 mixture of full, half, and third energy components compared with the case in which all the injected D^0 beam is

at 120 keV. Q is increased by 100% and the pulse is not limited by impurity effects.

4. Variation with angle of injection:

Within limits the beam may be aimed at a sharper angle to the plasma to reduce the path length required to penetrate to the core. Figures 6a,b show cases where the beam radius of tangency is 250 and 220 cm, respectively. Some delay in the onset of the instability is won, but Q and neutron energy production vary little.

These cases serve to illustrate the sensitivity of this process to changes in plasma variables. It is important to note that these variables may be fixed by other constraints, such as the efficiency of discharge cleaning (for initial low-Z content), the success of ion source species control, and the design of neutral beam line systems (for angle of injection).

Wall-limiter materials other than SS/tungsten or molybdenum have not been widely used in tokamaks, and so it is of interest to determine the sensitivity of the beam-trapping process to the use of different materials.

IV. MATERIALS

As noted in Section II we use a simplified model for the charge exchange sputtering process for these sensitivity studies. As for sputtering yields, we have adapted the data recently reported by Behrisch, et al. [17]. The table shows the range of assumed values for $\bar{Y}$ for the materials we consider.

Figures 7a,b show the comparison of C, S_iC, F_e, M_o, W for the TFTR case discussed in Section III. While there are uncertainties in the measured sputtering yields, and only preliminary results in the validity of the neo-classical inward diffusion assumption [18] we see that the best results are obtained for the low-Z, low sputtering pyrolytic graphite and S_iC reported by Behrisch. The reduction of impurity effects by choice of materials could well ease the constraints on power supplies, beam line design and species control imposed in other areas.

TABLE: Values for $\overline{\overline{Y}}$

Material	$\overline{\overline{Y}}$ (#/eV)
SS	2.10^{-6}
C^{+}	1.10^{-6}
S_iC [16]	2.10^{-6}
M_o	$1.4\ 10^{-6}$
W	$1.6\ 10^{-7}$

[+]Pyrolytic graphite sample (Union Carbide) quoted by Behrisch [17].

References

[1] J. T. Hogan, J. F. Clarke, J. Nucl. Mater., 53, 1 (1974).

[2] E. Hinnov, J. Nucl. Mater., 53, 9 (1974).

[3] L. A. Berry, et.al., Plasma Physics and Controlled Nuclear Fusion, Fifth Conference Proceedings, Tokyo, 1974. IAEA CN-33/A5-2, p.113.

[4] K. Bol, et.al., Plasma Physics and Controlled Nuclear Fusion, Fifth Conference Proceedings, Tokyo, 1974. IAEA CN-33/A4-1, p. 77.

[5] J. A. Rome, J. F. Clarke, J. D. Callen, Nuclear Fusion 14, 141 (1974).

[6] A. C. Riviere, Nuclear Fusion 11, 363 (1971).

[7] R. L. Freeman, E. M. Jones, Culham Laboratory Report CLM-R137, 1974.

[8] J. P. Girard, D. A. Marty, P. Moriette, Plasma Physics and Controlled Nuclear Fusion, Fifth Conference Proceedings, Tokyo, 1974. IAEA CN-33/A17-2, p. 681.

[9] H. P. Furth, private communication.

[10] J. T. Hogan, Oak Ridge National Laboratory Report ORNL-TM-5153, 1975 (to be published in Methods of Computational Physics, Vol. 16).

[11] J. T. Hogan, R. H. Fowler, H. C. Howe, Proc. 7th Conf. on Numerical Simulation of Plasmas, Courant Institute, New York, 1975.

[12] J. K. Munro, et.al., Oak Ridge National Laboratory Report, ORNL-TM-3262, 1976.

[13] J. D. Callen, et.al., Plasma Physics and Controlled Nuclear Fusion, Fifth Conference Proceedings, Tokyo, 1974. IAEA CN-33/A16-3, p. 645.

[14] P. H. Rutherford, Phys. Flu. 17, 1782 (1974).

[15] C. Jordan, Mon. Not. Royal Astron. Soc., 142, 501 (1969).

[16] W. Tang, et.al., Phys. Rev. Lett. 35, 660 (1975).

[17] N. R. Behrisch, B. B. Kadomtsev, Plasma Physics and Controlled Nuclear Fusion, Fifth Conference Proceedings, Tokyo, 1974. IAEA CN-33/S2, 229.

[18] S. A. Cohen, J. L. Cecchi, A. S. Marmar, Phys. Rev. Lett. 35, 1507 (1975).

* Research sponsored by the U. S. Energy Research and Development Administration under contract with the Union Carbide Corporation.

Figure Captions

Fig. 1: Schematic view of the energy deposition-impurity production process. The beam slows from its initial energy in a time τ_s, thereby delivering E_{plasma}. This energy is confined for a time τ_E, before being released to the wall. There the impurity production rate $\dot{N}_Z(a)$ is started, and after an inward impurity diffusion time τ_d^Z, the impurities arrive in the plasma core. The Q value rises on the beam slowing time scale however, and values near unity can be achieved before $N_Z(0)$ is significant.

Fig. 2: The charge exchange sputtering process for H-Au is examined with fixed plasma profiles. As machine size increases by a factor 5 in minor radius, the number of impurities produced per eV of charge exchange loss varies by 20%. The charge exchange flux varies by 10%, while the central neutral density drops by a factor 15.

Fig. 3: The TFTR configuration we adopt as a standard case has these parameters:

a_{plasma} 54 cm	I 1 MA
$a_{limiter}$ 85 cm	$T_e, T_i(0)$ 4 keV
R_0 248 cm	$N_e(0,0)$ $7.10^{13}cm^{-3}$
B_T(axis) 50 kG	$N_0(0,0)$ $1.4\ 10^{12}cm^{-3}$
	$N_{Fe}(0,0)$ $3.5\ 10^{10}cm^{-3}$

[3a]: The evolution of T_e and T_i. Impurity trapping causes preferential heating near the edge.

[3b]: Electron density evolution. Cold external neutral gas and the plasma evolution from the initial isolated state create an inverted density profile in a region of low T_e.

[3c]: The iron diffusion is hindered by the cold plasma blanket, but after about 200 msec substantial diffusion into the plasma core occurs.

[3d]: The beam deposition profile for the 120 keV D_0 shows the progression from strongly peaked deposition to edge heating.

[3e]: The half and third energy components penetrate very weakly. H(0) values of 1 or 2 are acceptable initially, but within 100 msec the instability develops.

[3f]: Ion temperatures reach 7 keV before falling, the Q value peaks at .36 while neutron output exceeds 1.8 MJ.

Fig. 4: The standard case is revised to include an 8% initial oxygen content. The Q and W_N values change by less than 20%, but there is no bulk heating of the thermal ions.

Fig. 5: If the beam were to be composed solely of 120 keV deuterons, the Q and W_N values would increase. The greater bulk heating of ions is prevented by onset of the beam trapping instability.

Fig. 6: Steepening the entrance angle for near-parallel injection produces a slight enhancement of T_i, and a slightly longer pulse length.

Fig. 7: A survey of materials is complicated by the absence of needed information about sputtering thresholds and yields, and about the radiative properties of highly stripped heavy metals. Nonetheless, the relative advantages of low-Z and low maximum yield can be compared with metals with higher Z and low yield. The variation with material produces a factor 2 improvement in deposition at 300 msec, and the low-Z candidate would produce long pulses if pessimistic impurity diffusion assumptions were relaxed.

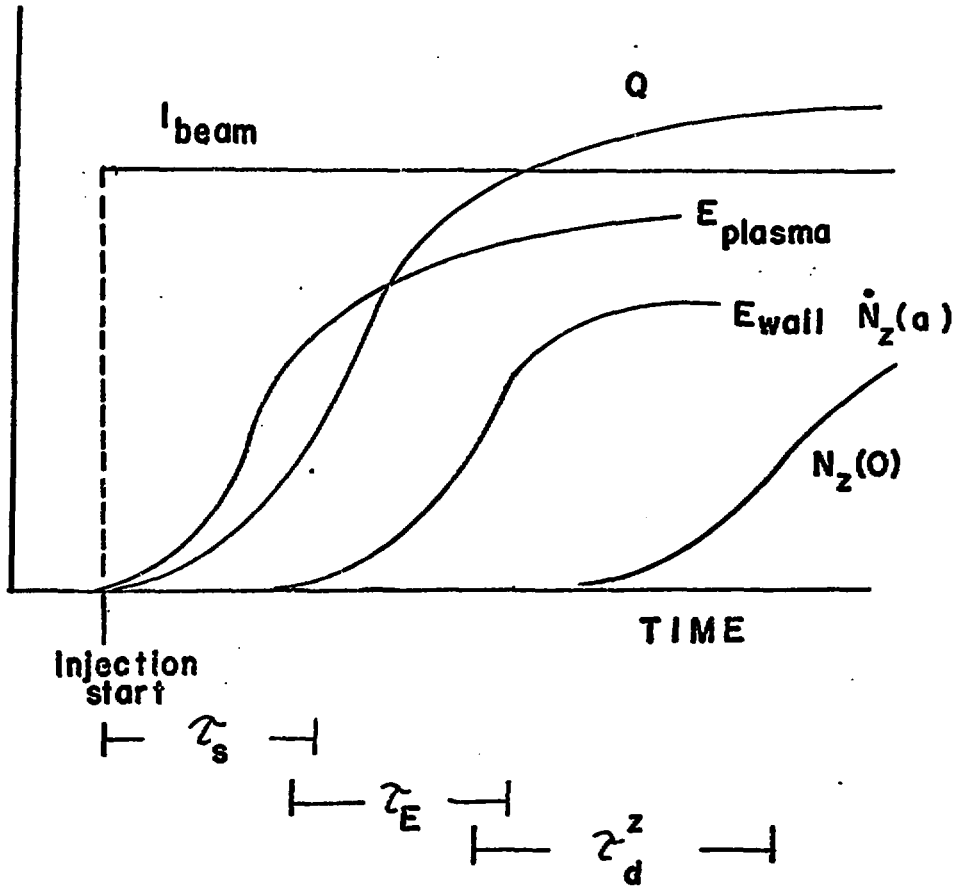
Q
I_{beam}
E_{plasma}
E_{wall} $\dot{N}_z(a)$
$N_z(0)$
TIME
Injection start
τ_s
τ_E
τ_d^z

Fig. 1

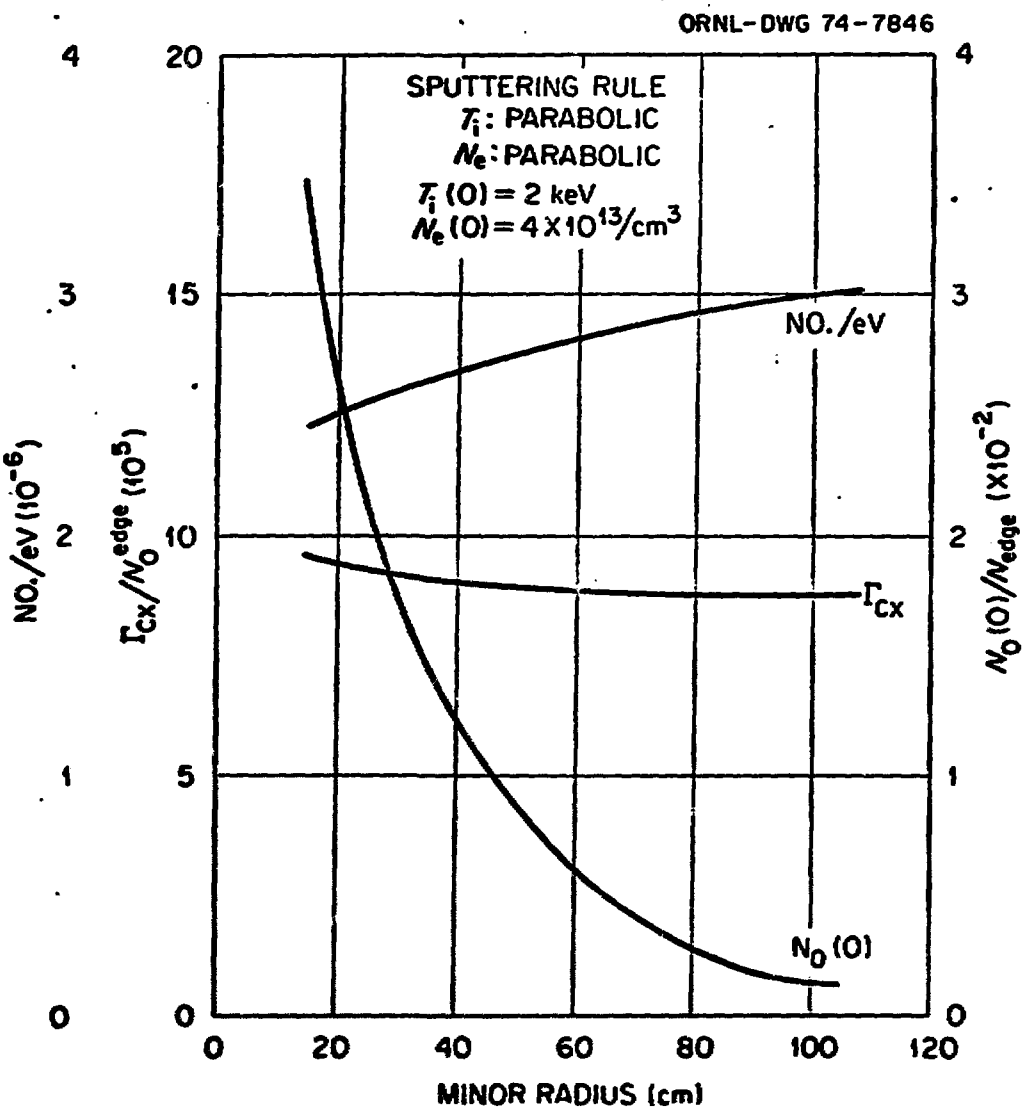
ORNL-DWG 74-7846
SPUTTERING RULE
T_i: PARABOLIC
N_e: PARABOLIC
$T_i(0) = 2$ keV
$N_e(0) = 4 \times 10^{13}/cm^3$
NO./eV
Γ_{cx}
$N_0(0)$
NO./eV (10^{-6})
Γ_{cx}/N_0^{edge} (10^5)
$N_0(0)/N_{edge}$ ($\times 10^{-2}$)
MINOR RADIUS (cm)
0
20
40
60
80
100
120
0
5
10
15
20
0
1
2
3
4

Fig. 2

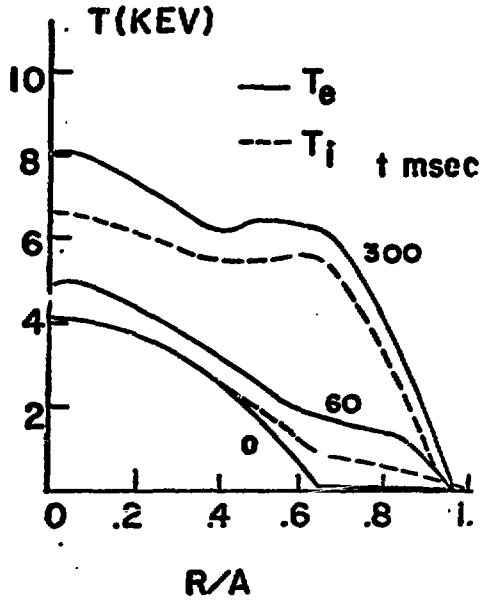

Fig. 3a

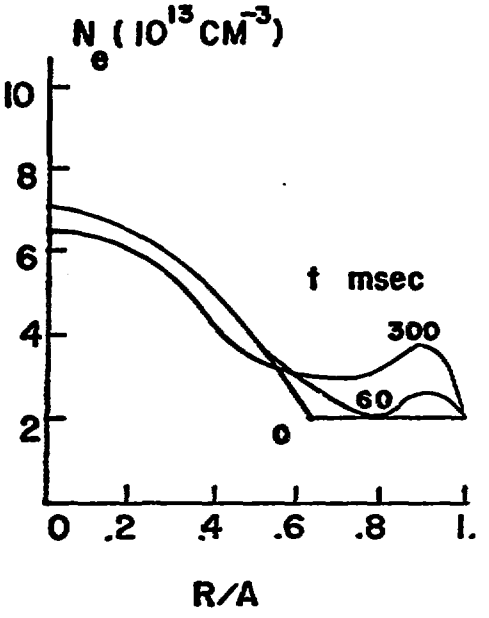

Fig. 3b

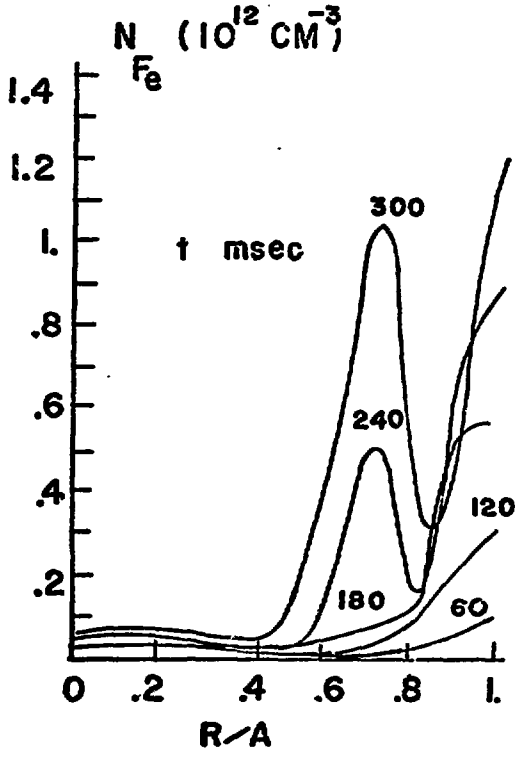

Fig. 3c

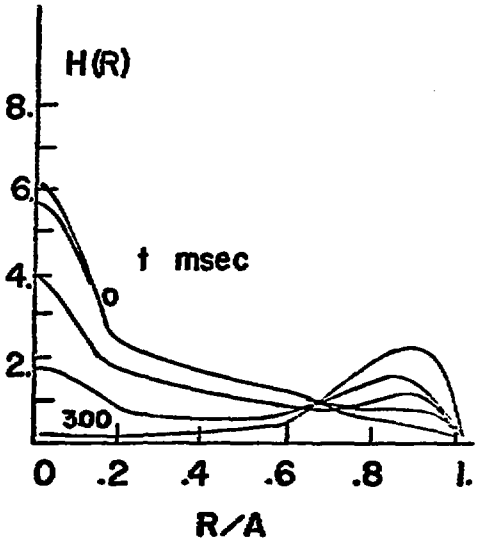

Fig. 3d

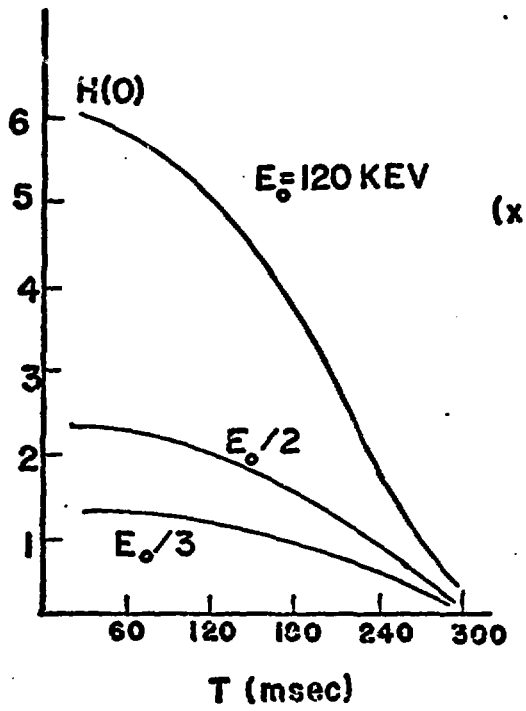

Fig. 3e

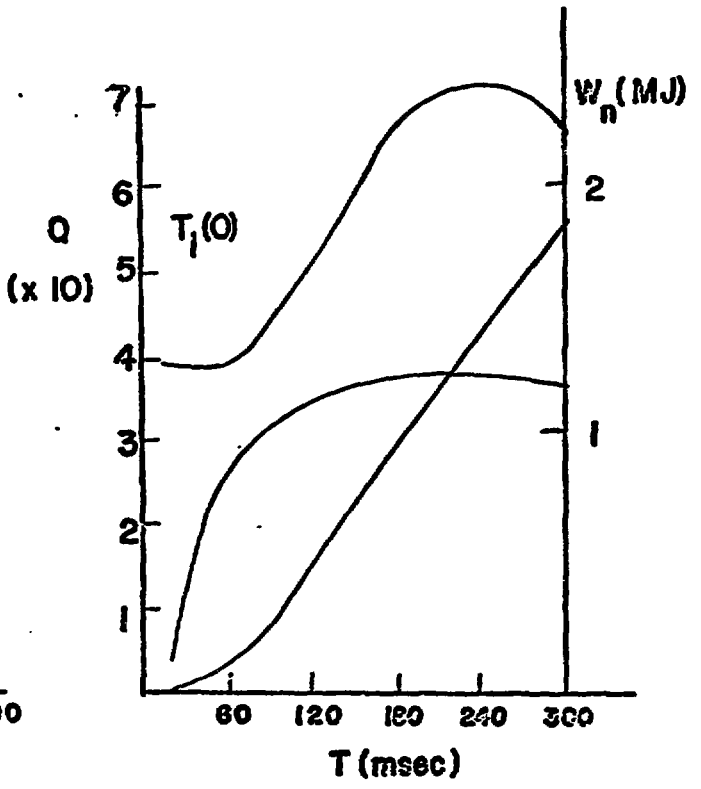

Fig. 3f

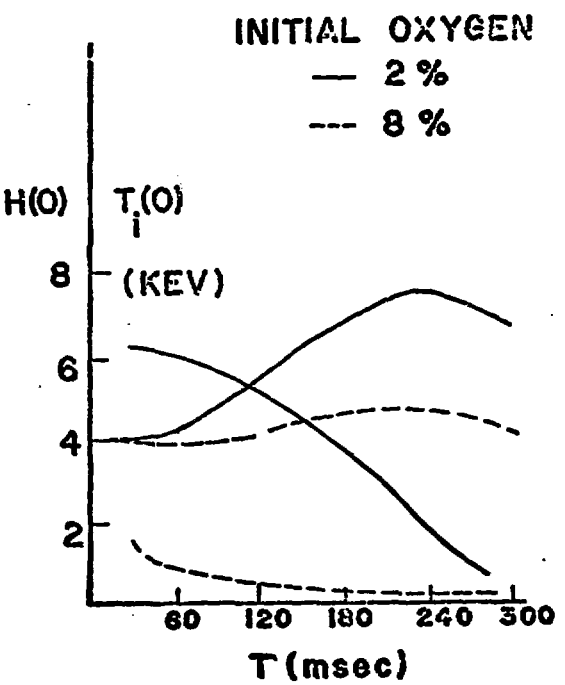

Fig. 4a

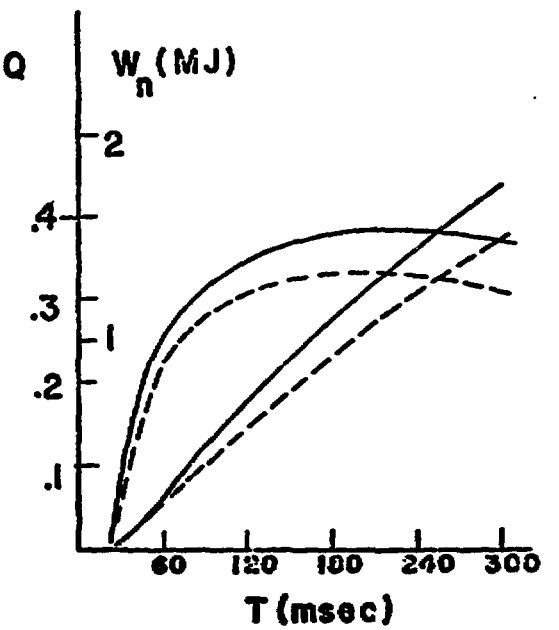

Fig. 4b

BEAM COMPOSITION

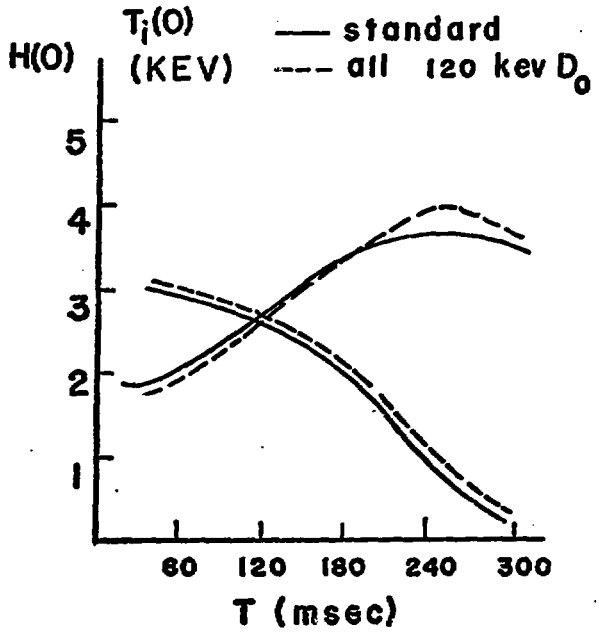

Fig. 5a

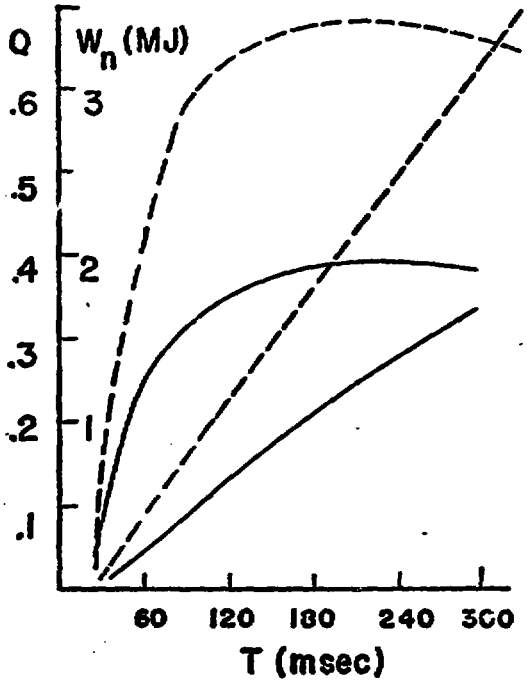

Fig. 5b

ENTRANCE ANGLE

— R_c = 220 cm

--- R_c = 250 cm

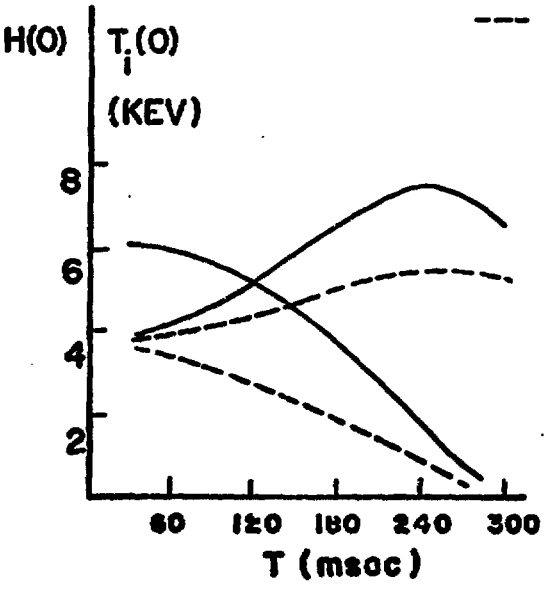

Fig. 6a

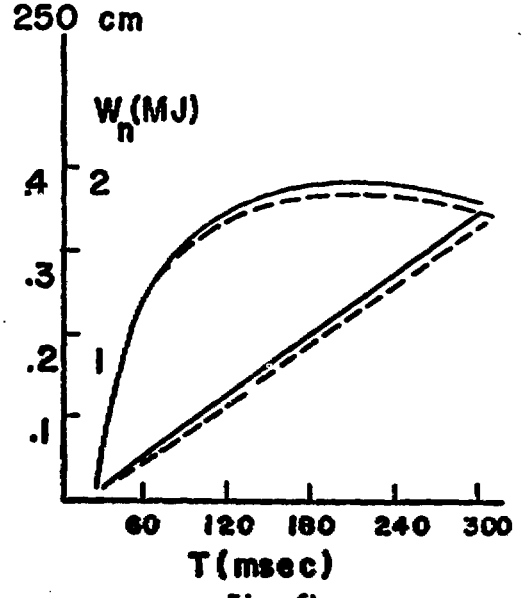

Fig. 6b

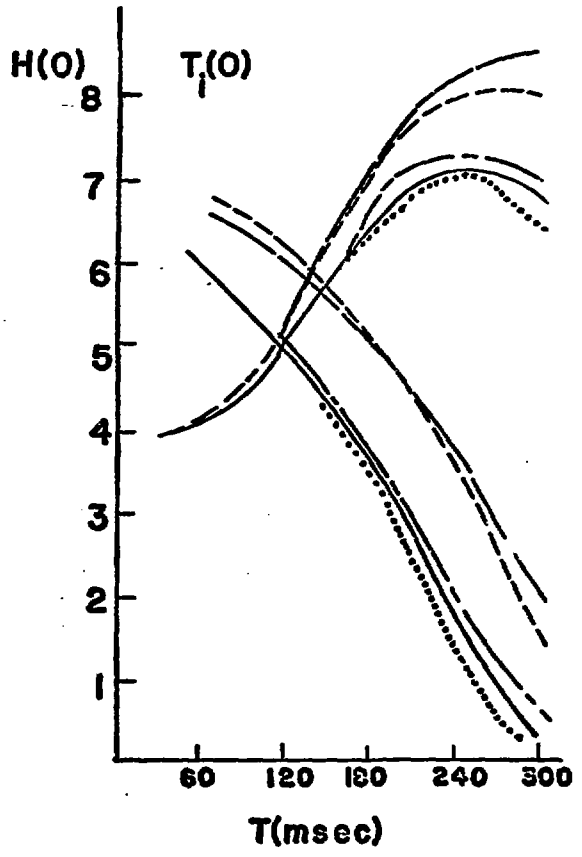

Fig. 7a

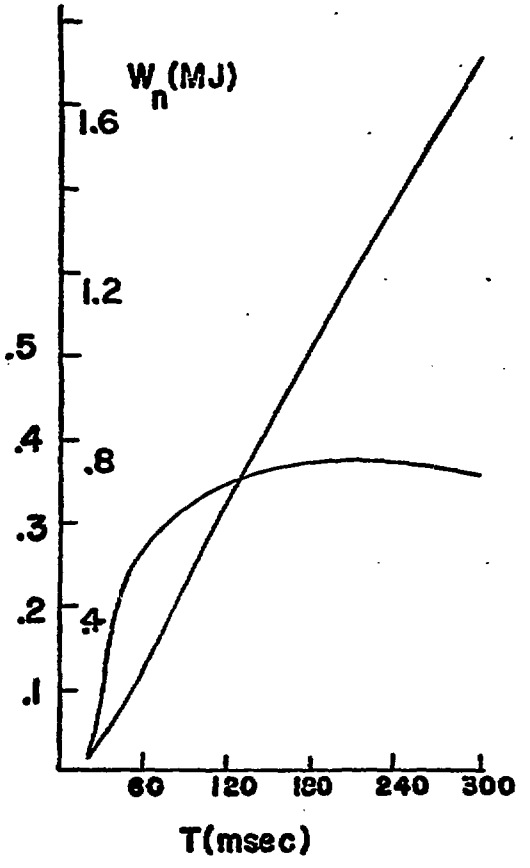

Fig. 7b

MATERIALS STUDY

——— IRON
- - - - - CARBON
—— Si C
····· MOLYBDENUM
—·— TUNGSTEN